THE JOURNAL OF PHYSICAL CHEMISTRY C

Article

pubs.acs.org/JPCC

Thermal Properties of Co/Au Nanoalloys and Comparison of Different Computer Simulation Techniques

A. Rapallo,[†] J. A. Olmos-Asar,[§] O. A. Oviedo,[§] M. Ludueña,[§] R. Ferrando,[‡] and M. M. Mariscal[§,*]

[†]ISMAC-Istituto per lo Studio delle Macromolecole del CNR, Via E. Bassini 15, 20133 Milano, Italy

[‡]Dipartimento di Fisica, Universita di Genova, and IMEM/CNR, Via Dodecaneso 33, 16146 Genova, Italy

[§]INFIQC/CONICET, Departamento de Matemática y Física, Facultad de Ciencias Químicas, Universidad Nacional de Córdoba, (X5000HUA) Córdoba, Argentina

ABSTRACT: In this work we investigate the performance of several simulation techniques, i.e., Canonical Molecular Dynamics, Canonical Monte Carlo, and the Optimized Multicanonical Monte Carlo, to study melting-like transitions of Co/Au nanoalloys that are compared to those of pure Co and Au clusters of the same size. A surprising enhancement in the thermal stability of core/shell $Co_{13}Au_{42}$ is observed compared to both pure clusters of the same size and shape. The novel property is analyzed using energetic and vibrational contributions throughout a detailed microscopic dynamic analysis.

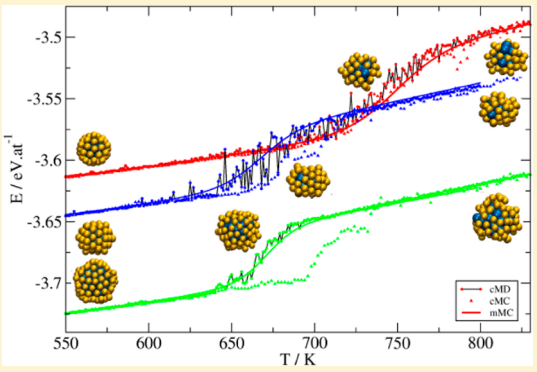

I. INTRODUCTION

In recent years the study of small metal clusters and nanoparticles has been the focus of several research areas, such as catalysis, solid-state physics, chemical-physics, biomedicine, and optics, to mention only some outstanding applications.[1]

Very recently, much effort has been devoted toward the possible use of metallic nanoparticles in biomedicine.[2−5] It is well established now that the strong optical absorption and scattering of metallic nanoparticles is due to the localized surface plasmon resonance,[6] a phenomenon which opens frontiers to the development of novel biomedical applications. The resonant extinction, which can be tuned to the near-infrared (nIR), allows the metallic nanoparticles to act as molecular contrast agents in a spectral region where tissue is relatively transparent. The localized heating due to resonant absorption, also tunable into the nIR, enables new thermal ablation therapies and drug delivery mechanisms.[7] The use of bimetallic nanoparticles with a core−shell configuration will enhance strongly the possibilities of a practical use of the resonant extinction. For instance, nanoparticles with a core−shell configuration where the magnetic core (i.e., Co, Ni, and Fe) is coated by a shell layer of a material which is biocompatible (i.e., Au) can present a more robust structure, so that they are very promising advanced materials.[8−16] Such structures are useful for studying proximity effects and structure stabilization, as the shell (Au) can protect the core (Co) from oxidation. Additionally, the shell provides a platform for surface modification and/or a further functionalization (i.e., thiolated-DNA and protein adsorption), linking magnetic properties and biocompatibility.[17]

Thermal stability is one of the basic requirements for a nanoparticle to be used in biological applications. It is therefore of crucial importance to study the thermal behavior of pure metallic nanoparticles as well as of binary metallic particles, the latter being in the core−shell configuration. One of the most important issues to be studied is the melting behavior, i.e. the solid−liquid phase transition. Metal nanoparticles usually have a much lower melting temperature than the corresponding bulk metals due to large surface-to-volume ratio. A common phenomenon observed by both experimentally and by means of theoretical calculations is that the melting point decreases with decreasing particle size.[18−21]

The study of the melting of nanoalloys depending on their size and composition has gained increasing attention in the past few years. From a theoretical viewpoint, melting of pure metal nanoparticles and nanoalloys has been studied by classical thermodynamic methods (see ref 1 and references therein). Many of these studies have employed computer simulations methods, which are very well suited to analyze the melting process in detail. In particular, the atomic structure and the energetic contributions can be extracted during the simulations in simultaneous. Many simulations have shown that nanoalloys may undergo complex structural transformations before complete melting (see ref 1). For example, with increasing temperature nanoalloys may fluctuate between homotops, keeping their overall geometric structure fixed. In addition, surface melting and/or demixing may also occur with increasing

Received: February 29, 2012
Revised: July 16, 2012

   dx.doi.org/10.1021/jp302001c | J. Phys. Chem. C XXXX, XXX, XXX−XXX

temperature before the complete melting of the whole nanoparticle.

The most common simulation methods in this field are canonical Monte Carlo (cMC) and canonical molecular dynamics (cMD). Both have been widely used in simulating the melting of nanoalloys and of nanoparticles in general. However, a comparison of these different simulation techniques is missing or only scarcely developed in the literature.

In the present work we choose Co, Au, and Co/Au nanoalloys as model systems, because of the great interest in them for applications in different fields. Cobalt-containing nanoparticles are chemically reactive and ferromagnetic. Joining gold with cobalt, we expect to obtain core−shell structures, with a cobalt core and a gold shell, because these metals mix very weakly in bulk and gold has a lower surface energy. In these core−shell structures, a much less reactive and much more biocompatible metal is in contact with the external environment, while the Co core still retains its magnetic properties.

From the point of view of the bulk materials, Au and Co present a marked difference in melting temperatures: 1337 (Au) and 1768 K (Co) which makes the study of their core−shell nanoalloys even more attractive. The present paper is structured as follows. In section II the methodological background and computational details are outlined. The results and their analysis are presented in section III. section IV contains the discussion and conclusion.

II. METHODOLOGIES AND COMPUTATIONAL TECHNIQUES

In all simulation techniques that will be used in the following, the interactions between atoms are modeled by a potential derived within the second-moment approximation of the tight binding model (SMTB).[22] Within this model, the potential energy is calculated as follow:

$$E_{\mathrm{tot}} = \sum_i \left(\sum_j A_{\alpha\beta} \mathrm{e}^{-p_{\alpha\beta}(r_{ij}/r_0^{\alpha\beta}-1)} - \sqrt{\sum_j \xi_{\alpha\beta}^2 \mathrm{e}^{-2q_{\alpha\beta}(r_{ij}/r_0^{\alpha\beta}-1)}} \right) \quad (1)$$

The first term on the right-hand side represents the atomic repulsion at short distances and the second one the attractive part of the potential. The SMTB potential parameters for Co−Co, Au−Au, and Co−Au that are used in most of the simulations are listed in Table 1. These parameters are taken from ref 23. Another set of parameters for the Co−Co interactions (taken from ref 24) has been used to check the results in some cases. We note that both parameter sets are able to reproduce the correct stability of anti-Mackay and chiral icosahedra in agreement with density-functional calculations.[25]

Table 1. SMTB Potential Parameters Used for Au−Au, Co−Co, and Au−Co Interactions (from refs 23 and 24)

	Au−Au	Co−Co	Au−Co
A/eV	0.210	0.189	0.141
ξ/eV	1.818	1.907	1.614
p	10.35	8.80	10.66
q	4.178	2.960	3.113
r_0/Å	4.073	3.620	3.850

Global Optimization Searches. Global optimization searches were used to look for the lowest-energy structures at the given sizes and compositions. The global-optimization algorithm is basin hopping and its variants, as detailed in refs 26 and 27.

Canonical Molecular Dynamics (cMD). Molecular dynamics simulations were performed by a homemade code in the canonical ensemble (NVT). Temperature is controlled by the Andersen thermostat. The equations of motion were solved by the Velocity Verlet algorithm, with a time step of 5 fs.

In most cases, the heating rate was of 1 K/ns. Slower rates have been used in some cases to check the convergence of the results. All reported cMD caloric curves are the result of an average of at least ten independent runs. Each run starts from the lowest energy structure found by the global minimization searches.

Canonical Monte Carlo (cMC). In this case, the simulations were carried out by means of an off-lattice Monte Carlo algorithm in the canonical scheme, where the positions of the atoms were allowed to change. Unlike in the case of lattice models, where atoms may assume only certain positions in a pregiven lattice, in this type of simulations the atoms can access any point in space. The only restriction applied to their motion is given by the transition probability between the initial and final state as prescribed by Metropolis algorithm.[28] "Short-jumps" allow description of the vibrational motion of all atoms in the neighborhood of their equilibrium positions.[29]

The number of particles N and the volume V were fixed all through the simulations and the temperature T was allowed to increase from 1×10^{-4} K until 1000 K in 500 steps of 30000 MC-step each. Thus, in this stepwise procedure the system explored the configuration space at different temperatures, allowing the accumulation of the average potential energy and its fluctuation with temperature. A total of ten independent simulations were averaged for each melting run, all starting from the lowest energy structure found by global optimization.

Optimized Multicanonical Monte Carlo (mMC). A more sophisticated Monte Carlo method has been also implemented. This will be denoted in the following as optimized multicanonical Monte Carlo (mMC). This method combines the Trebst et al. optimization of the ensembles for equilibration in broad-histogram Monte Carlo simulations[30] with the multicanonical algorithm.[31] In our method the conformational sampling of the system is obtained through a hybrid Monte Carlo procedure, where the move is done by the molecular dynamics, in an unphysical statistical ensemble which adopts, instead of the Boltzmann weight, an artificial one ensuring maximum number of roundtrips between low (E_-) and high (E_+) potential energy (E) values per unit computer time.[30] According to Trebst et al.,[30] a certain weight $w(E)$ in a general ensemble, defining the acceptance probabilities for moves based on the standard Metropolis scheme

$$p(E \rightarrow E') = \min\left(1, \frac{w(E')}{w(E)}\right) \quad (2)$$

is preliminarily necessary to be able to sample all the system's energy range of interest (E_-,E_+). With the aid of this weight a Monte Carlo simulation is performed and three histograms are collected: the histogram H of the potential energy E and the histograms H_- and H_+ of the so-called "labeled walker". This simply means that the sampled energy values contribute to the histogram H_- until the value E_+ is reached. Since then the histogram H_+ is updated instead of H_- until the value E_- is reached again and H_- begins to be further updated instead of

dx.doi.org/10.1021/jp302001c | J. Phys. Chem. C XXXX, XXX, XXX−XXX

H_+, and so on. During the simulation a convenient number of roundtrips in (E_-,E_+) must be realized to form accurate histograms H_- and H_+. Trebst et al. considered the random walk in energy as a diffusion process in the energy space, and developed an analytical procedure to optimize the flow of the sampling process across the energy range so as to maximize the roundtrip rate, by using a Fick's law formalism, and relating the optimal sampling distribution to the local diffusivity profile.[30] In such a way they obtained a recipe for building the optimal biasing weight in an iterative fashion by using the above-mentioned energy histograms. The result of their analysis is that given the starting $w(E)$, a better weight is obtained by

$$w'(E) = w(E)\sqrt{\frac{1}{H(E)}\frac{\mathrm{d}f(E)}{\mathrm{d}E}} \tag{3}$$

where $f(E)$ is given by

$$f(E) = \frac{H_+(E)}{H_+(E) + H_-(E)} \tag{4}$$

With the new weight $w'(E)$ a new run can be performed and eqs 3 and 4 used to obtain an even better weight. After a certain number of iterations the optimal weight will be at convergence and the random walker will perform the maximum number of roundtrips per given computer time in (E_-,E_+). From the point of view of the systems we are interested in, maximizing the number of roundtrips helps in escaping more efficiently from the different local minima and funnels in the potential energy surface, thus ensuring the most complete sampling of the energy landscape for a given computational time. Further, since maximizing the roundtrip speed implies spending more time in those regions of the energy landscape where the diffusivity is low,[30] the method ensures more thorough sampling of the energy landscape's bottlenecks, corresponding to the regions where phase transitions take place, which are very delicate to be accurately sampled. Though very appealing, this method is not self-sufficient since it requires a starting weight allowing for the sampling of the entire range (E_-,E_+) to be known. In the case of nanoclusters and nanoalloys this means that a weight must be available to sample from energy E_- pertaining to zero Kelvin (the energy of the global minimum), or to any temperature below the relevant phase transitions we want to study, to some energy E_+ well above the melting point of the system. Of course this weight is not known, and if it is so, the complete thermodynamic of the system should be already solved. For systems of moderate complexity, this weight can be constructed by means of some generalized ensemble technique such as parallel tempering,[32] Wang–Landau algorithm,[33] $1/k$ sampling,[34] multicanonical method,[31] and so on. Moreover the thermodynamic properties can be calculated directly by reweighting from those weights without resorting to the optimization of the ensemble. Anyway, it is known[35,36] that these methods in their basic formulation run into troubles if the system's energy landscape presents a very complex topography though narrow bottlenecks, multiple minima, and multifunnel structure, which is the case of metallic nanoclusters and nanoalloys, since they experience dramatic slowdown in crossing the phase transition regions of the potential energy surfaces, and the "tunneling times" between low and high energies severely increase, thus leading to inefficient/inaccurate sampling of the whole energy spectrum. Our idea was then to take advantage of the capabilities of the generalized ensemble methods to build up the weights to sample wide ranges of the energy space, and contrast their difficulties in overcoming entropic barriers by means of the ensemble optimization[30] which speeds up the random walk in E by enhancing the sampling exactly in those critical regions of the potential energy landscape which make the generalized ensemble techniques to run in troubles. The multicanonical[31] and the ensemble optimization[30] techniques were then combined in an original protocol to build the weight and optimize it on the fly rather than applying each method sequentially, which could be impossible in the most complex cases. It is worth mentioning that the choice of the multicanonical method is not mandatory, and other methods could have been chosen as well. In the multicanonical method, a weight proportional to the reciprocal of the system's density of states is iteratively built up and used to sample the potential energy surface. The algorithm can be briefly described as follows: in a first iteration a standard canonical simulation at a high temperature T where the system is melted is performed and the histogram H^1 of the energy is collected. The visited energies will be in some range (E_0^1,E_1^1). Then a biased potential $E' = E + k_BT\ln[H^1(E)]$, (k_B being the Boltzmann constant), is used to perform a second iteration. Such a biased potential produces roughly a uniform sampling of the energy values in the range visited in the preceding iteration, and extends the new range of visited energies to a broader (E_0^2,E_1^2), containing the preceding range. Some technicalities are to be implemented so that the new visited energy range is extended only toward the lowest energies, the highest limit roughly remaining E_1^1, i.e., such that (E_0^2,E_1^1) is the new range with $E_0^2 < E_0^1$. The histogram H^2 of the energy is collected again and used to make a new bias for a further iteration with potential $E'' = E + k_BT\{\ln[H^1(E)] + \ln[H^2(E)]\}$ which will produce roughly uniform sampling in (E_0^2,E_1^1) and visits in a broader range (E_0^3,E_1^1) with $E_0^3 < E_0^2$. By proceeding in this way the whole energy spectrum of the system can be visited from the melt to ideally the global minimum, and the equilibrium thermodynamic of the system can be characterized as a function of the temperature. Indeed from the known bias and the system's configurations at all energies, reweighting procedures can be used to recover the physics of the systems at temperatures other than T used for the simulation.[32] Our method works exactly within this framework, but optimization of the ensemble is also introduced by collecting on the fly the histograms necessary to the Trebst et al. procedure and biasing the multicanonical weight by means of eqs 3 and 4 over the growing range of energies visited during the different iterations. To be more explicit, suppose the first iteration of the multicanonical method is completed and the multicanonical weight is built up in the sampled range (E_0^1,E_1^1). We can identify E_0^1 with E_-, and E_1^1 with E_+ and collect H, H_-, and H_+ while running the second iteration. At the end of the second iteration these histograms can be used to optimize the multicanonical weight in the range (E_0^1,E_1^1) by means of eqs 3 and 4, whereas the standard multicanonical weight is built up in (E_0^2,E_0^1). Running the third iteration with this composite weight will enhance the roundtrip speed in the range visited during the first iteration, while working as the standard multicanonical method below E_0^1. In particular the visited energy range will develop toward lower energies as desired. If we now identify E_0^2 with E_-, we can collect the quantities to optimize the weight over the range (E_0^2,E_1^1) visited during the second iteration. By proceeding in this way we can optimize the multicanonical weight over the growing energy range visited iteration by iteration, thus enjoying the advantages of both the multicanonical and

dx.doi.org/10.1021/jp302001c | J. Phys. Chem. C XXXX, XXX, XXX−XXX

optimized ensemble methods and overcoming the deficiencies of each one. Though both the algorithms adapted and combined in the original procedure proposed here are neither presented nor implemented as parallel techniques, the method described above, was given a parallel implementation so as to take advantage of multiprocessor computers and further improve the statistics by combining the results of different parallel runs. Essentially each processor works as described above, but the underlying multicanonical, optimized weights, and histograms are built up by combining the different processes' outcomes. All of the necessary histograms collected among the processes were combined through a procedure derived from the Fenwick's direct multiple histogram reweighting method.[37] According to this procedure the histograms coming from the different processes are weight-averaged, the weights being built up using the hypothesis that the update of a histogram follows the Poisson statistics. In this way the uncertainty for each bin in the histogram is a direct function of the number of hits in that bin, and both the weights and the average can be built up in one step with no more information than the available histograms.[37,38] The procedure was applied to the same pure and bimetallic clusters studied by means of MD and MC. All the runs employed 48 parallel processes (random walkers) and completed within 15 to 35 iterations, depending on the size of the systems. The number of MC steps was assigned to each iteration according to a geometric progression starting from a minimum value for the first iteration to a maximum one for the last. The number of MC steps per process necessary to complete the runs, ranged from 90 million for the smallest clusters to 250 million for the biggest ones. Since one MC steps corresponds, in our hybrid Monte Carlo algorithm, to one step of Molecular Dynamics, the computational burden given in terms of MC steps coincides with that given in terms of number of potential energy function evaluations.

III. RESULTS AND DISCUSSIONS

Pure Clusters. Caloric curves, i.e., potential energy as a function of temperature, were constructed for both Au and Co clusters of different sizes starting at low temperature from their global minimum, obtained through the basin-hopping algorithm, in the case of cMC and cMD.

In the macroscopic limit, these curves are a useful tool to monitor the occurrence of phase transitions, which imply a sudden jump in the energy with respect to the temperature. This occurs at the melting temperature T_m.

This strategy, however, is not suitable for a reliable estimate of the correct melting temperature in the nanoscopic limit, where it is more appropriate to speak of a melting temperature range. Small clusters and nanoparticles do not have a sharp phase transition. Instead, melting occurs over a finite interval of temperatures, although the width of the interval becomes smaller as the nanoparticles increase in size.[38]

In Figure 1 caloric curves for pure gold clusters of 55, 147, and 309 atoms are shown, as well as the global minima structures (insets). As it can be observed the well-known melting-point depression is captured using the three methods mentioned above. In general terms, a good agreement is found between all simulation techniques, in particular in the regions before and after the melting range. In the case of optimized mMC simulations, a more sudden jump in the curve is observed (see Au_{309}) and it appears at lower temperature. By construction mMC is able to perform many transitions across

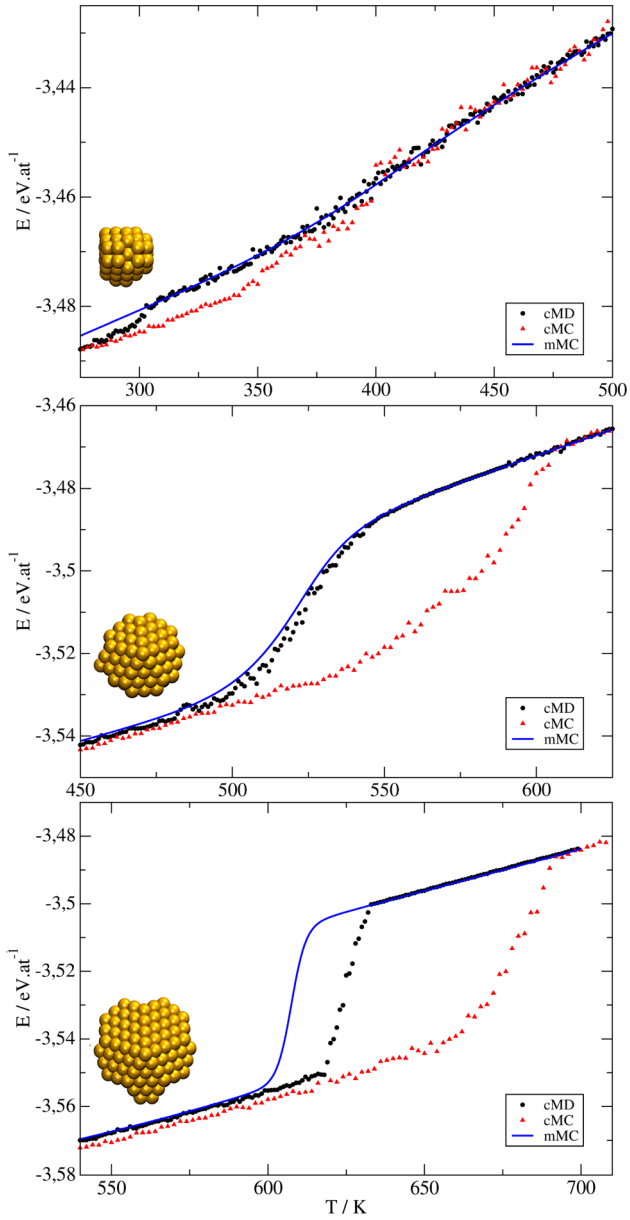

Figure 1. Caloric curves for Au clusters with N = 55, 147, and 309 atoms (from top to bottom), using cMD, cMC, and optimized mMC simulations. Initial structures corresponding to global minima are also shown in the inset.

the melting point during the simulation. This allows for an accurate sampling of the configurations on the potential energy surface (PES) contributing to the transition bottleneck, by allowing for the same degree of ergodicity at all energy levels. On other side, ergodicity of cMD and cMC is ideally reached with some infinite sampling, which is not the case of typical simulations. As can be observed in the caloric curves, for the largest system the melting range appears at different temperatures for the three methods, although the difference is relatively small, especially if we consider the model limitations for reproducing experimental melting temperatures. For studying the performance of cMD technique with the improvement in the sampling, we have varied the rate of heating from 1.00 to 0.01 K ns^{-1} for Au_{147} and from 1.00 to 0.10 K ns^{-1} for Au_{309}. Results are shown in Figure 2. As can be observed, the melting region moves to lower temperatures and

dx.doi.org/10.1021/jp302001c | J. Phys. Chem. C XXXX, XXX, XXX−XXX

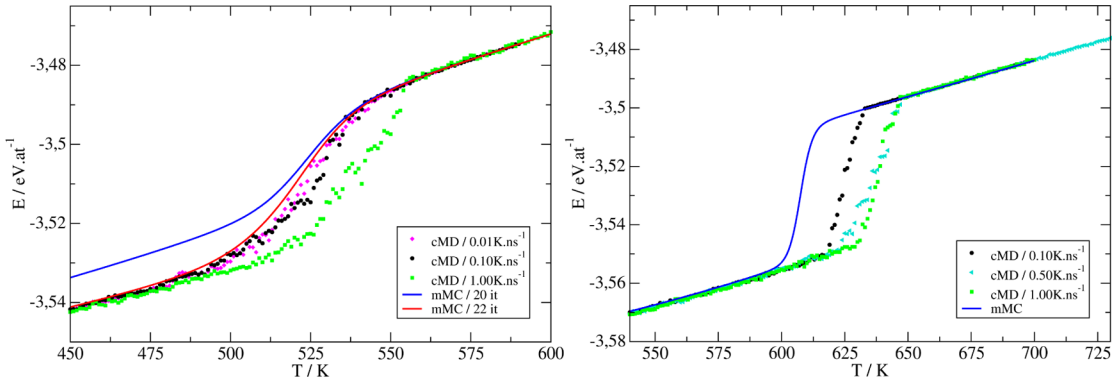

Figure 2. Comparison of the performance of mMC and cMD using different sampling, (a) Au_{147} and (b) Au_{309}.

gets closer to the value found with mMC as the rate of heating becomes smaller. This is due to the improvement in the sampling which allows a more complete exploration of the PES during the transition. The behavior of cMC algorithm is similar to cMD but with a slower convergence (not shown here). The implementation of new types of moves could accelerate that convergence.

On the other hand, for some systems mMC was not able to reach a global minimum structure without exploring the convergence as a function of the number of iterations, and configurations of higher energy were found for low temperatures, getting stuck into a small pool of all the available conformers (see blue curve in Figure 2a). Note however that, even in this case, both cMD and mMC agree very well for what concerns the melting temperatures. The main difference is that the jump in the caloric curve is larger in cMD than in mMC, because the former samples lower energy isomers at lower temperature, since it starts from the global minimum. If the number of iterations is increased in mMC for Au_{147}, a noticeable improvement of the results is obtained. We show in Figure 2a how increasing the number of iterations from 20 (blue curve) to 22 (red curve) and the quantity of parallel processors used from 24 to 48 yields better results, reaching now, at low temperatures, the lowest energy structure.

As in the case of pure gold clusters, for cobalt the jump in the melting curves increases with the size of the clusters, as expected for metals in the nanoscale (see Figure 3). It is interesting to note in this case the excellent agreement found between the three techniques during the range of temperatures before and after melting, and during the phase transition for small systems. However, significant differences are found in the region close to the melting-like, in particular for the largest cluster (Co_{309}). These differences could be attributed —in principle— to the different sampling procedures used to evaluate the energy of the systems, as we have pointed before. We can also see that the temperature at which melting process begins follows the same sequence as for pure gold clusters: mMC < cMD < cMC.

A fact that is worth mentioning is that in all cases the energy at low temperature is exactly the same (not shown in the curves), even in the case of mMC, for most of the systems, where the starting point is a canonical simulation at high temperature (above the melting point), whereas, in the case of cMD and cMC the starting points are the lowest-energy structures obtained with the basin-hopping algorithm. An extra capability of the mMC procedure is that there is no need to know the structure of the global minimum in advance to

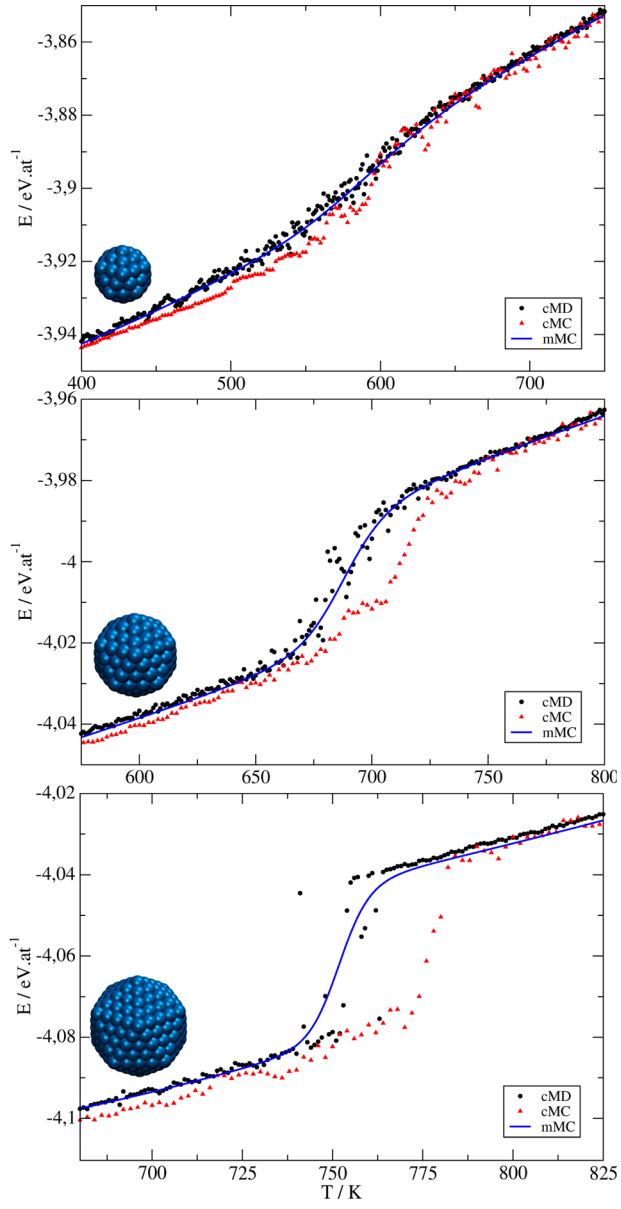

Figure 3. Caloric curves for Co clusters with N = 55, 147, and 309 atoms (from top to bottom), using cMD, cMC, and optimized mMC simulations. Initial structures corresponding to global minima are also shown in the inset.

dx.doi.org/10.1021/jp302001c | J. Phys. Chem. C XXXX, XXX, XXX−XXX

calculate the thermodynamic properties, such conformations being, eventually, a result of the iterative method.

Co/Au Nanoalloys. After global optimization calculations using the basin-hopping algorithm, in all cases, the tendency to form core−shell structures emerged very clearly (see Figure 4), even if the starting points for the calculation were randomly generated bimetallic clusters, without any specific structural motif.

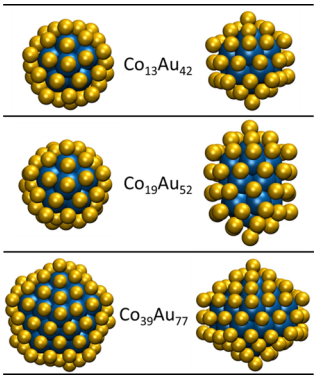

Figure 4. Final structures for the magic-number Co−Au nanoalloys after global optimizations.

The reorganization into core/shell structures occurs already at the early stages of the global-optimization runs. This result is interesting, as we have said, from a technological standpoint, since it suggests the effectiveness of gold as possible passivating agent. In the case of Co19Au52, a double icosahedron made of two 55-atom icosahedra sharing several atoms was found as the lowest-energy structure. Co39Au77 is of the icosahedral family. The Co core is a distorted fragment of an icosahedron of 55 atoms. It is distorted in such a way that there are no reflection symmetries (lack of any reflection plane) but it keeps a 5-fold symmetry axis. So, that it is a chiral structure of C_{5v} symmetry, which is however different from those which were found in ref 26. Also about the melting temperatures of the nanoalloys the results are interesting. Indeed the high value of this temperature indicates strong thermal stability of the compound, suggesting possible applications of these nanoalloys also in critical environmental conditions.

In Figure 5 the caloric curves are shown for the three nanoalloys considered. Again, a very good agreement is found for the three simulation techniques when clusters are relatively small (i.e., N = 55 atoms). However, when the number of atoms increases as well as the number of homotops,[39] a discrepancy between the different methods was observed. For instance, for the case of $Co_{39}Au_{77}$, cMC simulations show a jump in $E(T)$ at a relatively higher temperature. This could be an effect of the moves−trials implemented in the cMC code which are insufficient to sample the complex configurational space. However, an excellent agreement is found between cMD and mMC for $Co_{39}Au_{77}$.

In the case of optimized mMC simulations, with a number of iterations ranging from 15 for the smallest cluster to 35 for the largest one, it was possible to sample configurations that contribute to the properties down to temperatures below 200 K.

Another significant property that can be used to study the melting-like transition in detail is the heat capacity C_v, which

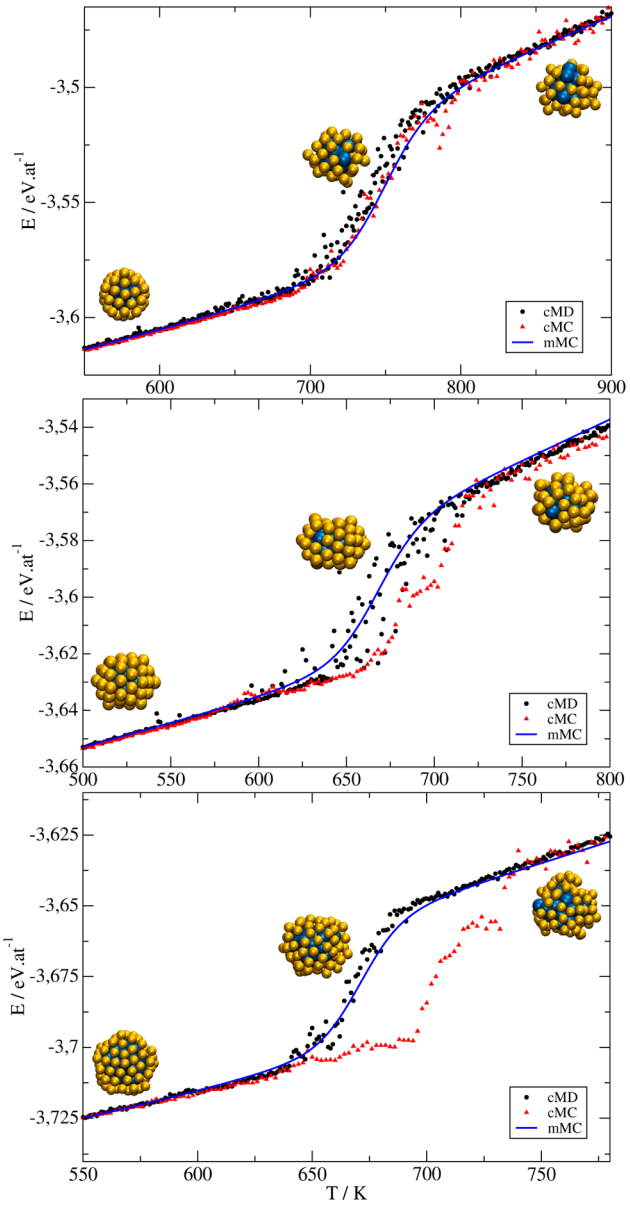

Figure 5. Caloric curves for nanoalloys with magic numbers N = 55, 71, and 116 (from top to bottom), using cMD, cMC, and optimized mMC simulations. Selected snapshots of the atomic configurations taken from the cMD simulations are shown.

can be defined as a function of the fluctuations in the potential energy as follows:

$$C_v = \frac{(\langle E^2\rangle - \langle E\rangle^2)}{k_B T^2} \quad (5)$$

where E is the potential energy, k_B is the Boltzmann constant, and T is the temperature.

In macroscopic systems, the melting point is defined as the temperature where the heat capacity C_v vs temperature diverges. It should be noted that in order to get correct values of C_v the variance $(\langle E^2\rangle - \langle E\rangle^2)$ should be uncorrelated. For this reason we have performed an exhaustive analysis of the correlation effect to ensure a good quality in the results of the heat capacity. Figure 6 shows the heat capacity for Au_{55}, Co_{55}, and $Co_{13}Au_{42}$ nanoalloy calculated with the three techniques. The quality of the results obtained by means of the mMC

dx.doi.org/10.1021/jp302001c | J. Phys. Chem. C XXXX, XXX, XXX−XXX

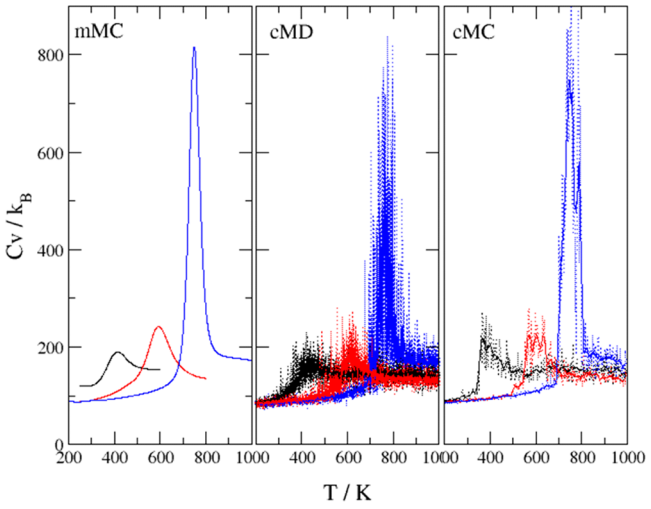

Figure 6. Heat capacity (C_v) for Au_{55} (black line), Co_{55} (red line), and $Co_{13}Au_{42}$ (blue line) nanoalloys using optimized mMC, cMD, and cMC simulations.

technique is evident. In the case of cMD and cMC large fluctuations are observed.

A separate analysis deserves the smallest cluster ($Co_{13}Au_{42}$) where the melting temperature is higher than that of the biggest ones (i.e., $Co_{19}Au_{52}$ and $Co_{39}Au_{77}$), and also significantly higher than that of both Au_{55} and Co_{55}. This fact is probably related to the particular stability that the "magic" geometry gives to that specific composition and size. In the case of nonmagic clusters, not represented here, the melting temperatures are even lower.

The fact that the mixed cluster $Co_{13}Au_{42}$ melts higher than both pure clusters is a quite surprising result, which shows significant differences compared to the results previously reported in the literature (see the discussion below). In order to check whether this result could be an artifact of our model, we have also run simulations with the Co−Co parameter set of ref 24 that have confirmed the same qualitative effect with minor quantitative differences.

Let us discuss our finding in comparison with the available results in literature. Previous simulations in different systems (AgCu, AgNi, and AuCu) have shown that doping an icosahedron with a single central impurity may increase significantly the melting temperatures even for quite large icosahedra. Mottet et al.[40] have shown that significant upward shifts of the melting point are achieved by putting a single Ni or Cu impurity in the central site of Ag icosahedra, for size up to 561 atoms. This effect was attributed to the strain release induced by the "small" central atom in the compressed central site of the icosahedron.

In the case of Cu/Au icosahedra an analogous effect was observed in cMC simulations by Cheng et al.,[41] who showed that the doping of icosahedral Au_{55} clusters with a single Cu atom can raise the melting point significantly, by up to 150 K, and the melting point of the three-shell $Cu_{12}Au_{43}$ cluster is 280 K higher than that of pure icosahedral Au_{55}. However in that case, the melting temperature of Cu_{55} was 780 K, indicating that the melting temperature of the $Cu_{12}Au_{43}$ three-shell structure is in the middle of both pure materials, as we can speculate a priori.

Finally, for $Ag_{27}Cu_7$ and $Ag_{27}Ni_7$, cMD simulations have shown melting temperatures that are higher than those of pure high-symmetry clusters at nearby sizes.[42] In this case the pure clusters also have a different symmetry than the nanoalloys. On the other hand, the pure clusters of the same size have a low symmetry and this causes a low melting point. In summary, the case of $Co_{13}Au_{42}$ is special because it is a high-symmetry nanoalloy which melts higher than the cluster of the more cohesive element (Co) that has the same size and the same type of high-symmetry.

The phonon density of state (DoS) is defined as the vibrational spectrum corresponding to a given system. In molecules, such spectrum is determined by vibrations of the individual bonds, it has a discrete nature, and it can be inferred via infrared (IR), Raman, and other spectroscopies. In bulk systems, the spectroscopic lines become broad bands, and systems of intermediate sizes such as clusters or nanoparticles have features ranging between those of the molecular and the extended systems.[43] The DoS function $S(\nu)$ was calculated using the microcanonical MD trajectories, in order to study the distribution of vibrational normal modes of the $Co_{13}Au_{42}$ nanoalloy system. The DoS function can be obtained from the Fourier transform of the velocity autocorrelation function $C(t)$

$$S(\nu) = \frac{2}{k_B T} \lim_{\tau \to \infty} \int_{-\tau}^{\tau} C(t) e^{-i2\pi\nu t} \, dt \tag{6}$$

where ν is the frequency and $C(t)$ is the velocity autocorrelation function.[44] A more detailed understanding into the microscopic dynamics could be appreciated analyzing the velocity autocorrelation function of a collection (α) of atoms, $C^{\alpha}(t)$ instead of the whole function. In this sense, the sets of atoms were chosen according to their coordination number (cn), in order to distinguish between core (cn > 10) and surface (cn < 10) atoms, considering only nearest-neighbors for the calculations of cn.

Therefore a set of DoS functions $S^{\alpha}(\nu)$ can be computed for all systems. This function reveals the vibrational behavior of the selected set of atoms.

Figure 7 shows the $S^{\alpha}(\nu)$ functions for Au_{55} and Co_{55} clusters computed at 200 K. Both DoS spectra showed a solid-like behavior due to the absence of density of states at zero frequency. Since the Au_{55} cluster at the global minimum does not present a high-symmetry structure, the DoS does not show noticeable distinguishing frequencies, as expected for any amorphous-like structure, in good agreement with previous results reported by Garzón et al.[45]

A different behavior is observed in the case of the Co_{55} cluster where three vibrational modes are clearly distinguished at high frequencies of the DoS. These normal modes correspond mainly to the vibration of inner atoms. Even more, both the core and shell atoms share the same characteristic frequencies.

Figure 7 (lower panel) shows the $S^{\alpha}(\nu)$ functions for the $Co_{13}Au_{42}$ nanoalloy. As can be observed the normal modes at high frequencies (corresponding to the core (Co) atoms) are decoupled from the normal modes of the shell ones (Au); that is, there are not shared frequencies, as can be observed for the case of Co_{55}, where at high and even at low frequencies there are several normal modes of the core and shell atoms with the same frequency. This effect could be responsible for the highest melting temperature of the nanoalloy with respect to the pure clusters of the same size. The Co_{13} core is stabilized by the presence of a Au_{42} shell. Since the Au_{42} shell does not have any normal mode of frequency similar to the Co_{13} core, the

dx.doi.org/10.1021/jp302001c | J. Phys. Chem. C XXXX, XXX, XXX−XXX

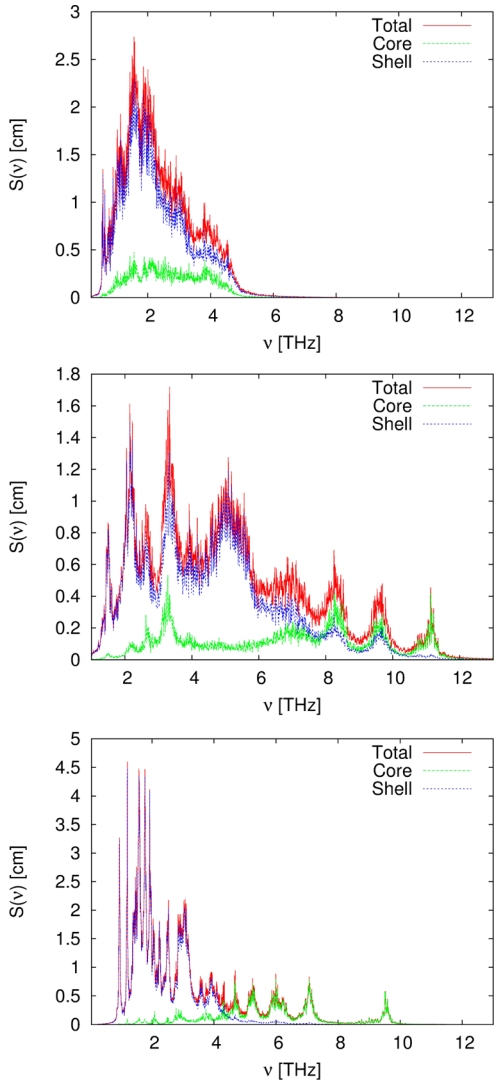

Figure 7. $S^{\alpha}(\nu)$ functions for Au_{55} (upper panel), Co_{55} (middle panel), and $Co_{13}Au_{42}$ nanoalloy (lower panel). Red full lines correspond to the total DoS, whereas the green and blues dotted lines represent the core and shell DoS, respectively.

subsystems cannot transfer efficiently the energy and therefore is thermally more stable than the pure ones.

Comparison of the Simulation Methods. As a summary, we can compare the performance and results obtained from the three techniques implemented in this work: cMD, cMC, and optimized mMC. In the case of cMD and cMC, the knowledge of the starting configuration is needed. At the initial stages of caloric curves, the sampling is highly limited by the low temperature, which confines the PES exploration in small regions of configuration space around the initial minimum. If the PES is multifunnel and simulation starts from a local minimum structure, it will be difficult to jump to a different funnel. If the structure of energy minimum is known, sampling is correct in the limit of low temperatures, so that a good performance can be obtained below and above the melting range. In the zone of the solid−liquid transition an exhaustive sampling is necessary if cMD or cMC are used, that implies slow heating rates for multifunnel PES especially for relatively large clusters in the case of cMD, or the inclusion of other types of trial moves, such as large jumps or exchanges in the case of cMC. In this case, the results obtained depend strongly on the quality of the sampling. If the PES is dominated by a single funnel, sampling is much easier and heating rates of 1 K/ns can be sufficient for clusters of several hundred atoms. For multifunnel PES and small sizes, even starting from a structure which is not the global minimum may lead to a correct description of the melting, because the cluster can rearrange to the lowest-energy configuration while heating. However this is not warranted, so that starting from the global minimum is recommended.

Optimized mMC has in principle the advantage of starting from a high temperature state, so no need of knowledge of the lowest energy structure is required. The sampling with this technique is broader, due to the smoothing of probability profile and subsequent reweighting of the states in the ensemble. Results in the melting region are more accurate, and much less noisy. By other hand, calculations with this methodology require higher computational resources and time. Moreover, mMC sometimes fails to find the lowest energy configuration if the number of iterations is not sufficient. The correct number of iterations is indeed rather difficult to decide a priori. In fact, in some cases we decided to increase the number of iterations of the mMC simulations because we already knew the global minimum structure, and we realized that the mMC simulation was not yet able to find it.

In summary, our results show that the study of the melting of nanoparticles and nanoalloys is a difficult problem, so that the use of different computational techniques is recommended in order to overcome the drawbacks that each of them would present if used alone. In particular, a pre-exploration of the low-energy part of the PES by some global optimization tool seems to be necessary in any case. For cMD and cMC, global optimization is necessary to give the correct starting configuration. In the case of mMC, global optimization is recommended because it gives reference results that are useful to understand whether a sufficient sampling has been obtained at low temperatures, below the melting range.

IV. CONCLUSIONS

We presented a detailed analysis of the melting transition in pure Au and Co clusters as well as in Co/Au nanoalloys with core−shell structure. Three different simulation techniques were used to explore the melting transition. In general terms we observe good agreement between the techniques; however, some important differences are found in the temperature region close to the melting. The optimized multicanonical Monte Carlo technique seems to be the most appropriate to capture with high precision the melting point, but it is recommended to supplement it by global optimization searches to check the quality of sampling at low temperatures.

Finally, for Co/Au nanoalloys, a novel phenomenon was observed in particular for the $Co_{13}Au_{42}$ cluster, where an enhancement in the thermal stability, compared to both pure clusters of the same size, was detected. That is, the melting temperature of the $Co_{13}Au_{42}$ cluster is higher than those of the Au_{55} and even the Co_{55} clusters. Note that Co_{55} presents the same kind of high-symmetry icosahedral structure as $Co_{13}Au_{42}$ and it has a much stronger total binding energy than $Co_{13}Au_{42}$. To our knowledge, this enhancement of the melting temperature has never been observed before.

A novel property has been examined by analyzing the energy contributions from different group of atoms (core and shell). In this sense, we found that the 42 Au shell atoms in the $Co_{13}Au_{42}$

dx.doi.org/10.1021/jp302001c | J. Phys. Chem. C XXXX, XXX, XXX−XXX

cluster are energetically more stable than the corresponding atoms of the $Au_{13}Au_{42}$ pure cluster.

The vibrational density of state functions have been used to study the vibrational dynamics of the inner and surface atoms. In particular we have found in the $Co_{13}Au_{42}$ nanoalloy that the normal modes at high frequencies (corresponding to the core (Co) atoms) are decoupled from the normal modes of the shell atoms (Au). These findings constitute a motivation for further research.

AUTHOR INFORMATION

Corresponding Author

*E-mail: marcelo.mariscal@conicet.gov.ar.

Notes

The authors declare no competing financial interest.

ACKNOWLEDGMENTS

The authors thank CONICET and CNR for an International Cooperation program in the biennium 2009−2010, Secyt UNC, Program BID (PICT BICENTENARIO: 2010-123), PIP: 112-200801-000983 "Nanotechnology in silico" for financial support, COST Action MP0903 "Nanoalloys" and MinCyT-ABESTII. J.A.O.-A. and M.L. thank CONICET for the fellowships.

REFERENCES

(1) Ferrando, R.; Jellinek, J.; Johnston, R. L. *Chem. Rev.* **2008**, *108*, 845−910.
(2) Nel, A. E.; Mädler, L.; Velegol, D.; Xia, T.; Hoek, E. M. V.; Somasundaran, P.; Klaessig, F.; Castranova, V.; Thompson, M. *Nat. Mater.* **2009**, *8*, 543−557.
(3) Storhoff, J. J.; Mirkin, C. A. *Chem. Rev.* **1999**, *99*, 1849−1862.
(4) Chithrani, B. D. *Nano Lett.* **2006**, *6*, 662−668.
(5) Seok Seo, W.; Hyung Lee, J.; Sun, X.; Suzuki, Y.; Mann, D.; Liu, Z.; Terashima, M.; Yang, P. C.; McConnell, M. V.; Nishimura, D. G.; et al. *Nat. Mater.* **2006**, *5*, 971−976.
(6) Bozhevolnyi, S.; García-Vidal, F. *New J. Phys.* **2008**, *10*, 105001.
(7) Liao, H.; Nehl, C. L.; Hafner, J. H. *Nanomedicine* **2006**, *1*, 201−208.
(8) Kayal, S.; Vijayaraghavan Ramanujan, R. *J. Nanosci. Nanotechnol.* **2010**, *10*, 1−13.
(9) Bao, Y.; Calderon, H.; Krishnan, K. M. *J. Phys. Chem. C* **2007**, *111*, 1941−1944.
(10) Lee, W.-r.; Kim, M. G.; Choi, J.-r.; Park, J.-I.; Ko, S. J.; Oh, S. J.; Cheon, J. *J. Am. Chem. Soc.* **2005**, *127*, 16090−16097.
(11) Mayoral, A.; Mejía-Rosales, S.; Mariscal, M. M.; Pérez-Tijerina, E.; Yacamán, M. J. *Nanoscale* **2010**, *2*, 2647−2651.
(12) Lin, J.; Zhou, W.; Kumbhar, A.; Wiemann, J.; Fang, J.; Carpenter, E. E.; O'Connor, C. J. *J. Solid State Chem.* **2001**, *159*, 23−31.
(13) Cho, S.-J.; Kauzlarich, S. M.; Olamit, J.; Liu, K.; Grandjean, F.; Rebbouh, L; Long, G. J. *J. Appl. Phys.* **2004**, *95*, 6804−6806.
(14) Cushing, B. L.; Golub, V.; J. O'Connor, C. *J. Phys. Chem. Solids* **2004**, *65*, 825−829.
(15) Park, J.-I.; Cheon, J. *J. Am. Chem. Soc.* **2001**, *123*, 5743−5746.
(16) Park, J.-I.; Kim, M. G.; Jun, Y.-w.; Lee, J. S.; Lee, W.-r.; Cheon, J. *J. Am. Chem. Soc.* **2004**, *126*, 9072−9078.
(17) Krishnan, K. M. *IEEE Trans. Magn.* **2010**, *46*, 2523−2558.
(18) Buffat, Ph.; Borel, J.-P. *Phys. Rev. A* **1976**, *13*, 2287−2298.
(19) Makarov, G. N. *Phys.-Uspekhi* **2010**, *53*, 179−198.
(20) Hasegawat, M.; Hoshino, K.; Watabet, M. *J. Phys. F: Metal Phys.* **1980**, *10*, 619−635.
(21) Mirjalili, M.; Vahdati-Khaki, J. *J. Phys. Chem. Solids* **2008**, *69*, 2116−2123.
(22) Cleri, F.; Rosato, V. *Phys. Rev. B* **1993**, *48*, 22−33.
(23) Goyhenex, C.; Bulou, H.; Deville, J.-P.; Tréglia, G. *Phys. Rev. B* **1999**, *60*, 2781−2788.
(24) Rives, S.; Catherinot, A.; Dumas-Bouchiat, F.; Champeaux, C.; Videcoq, A.; Ferrando, R. *Phys. Rev. B* **2008**, *77*, 085407−085414.
(25) Bochicchio, D.; Ferrando, R. *Nano Lett.* **2010**, *10*, 4211−4216.
(26) Rossi, G.; Ferrando, R. *Chem. Phys. Lett.* **2006**, *423*, 17−22.
(27) Rossi, G.; Ferrando, R. *J. Phys.: Condens. Matter* **2009**, *21*, 084208.
(28) Allen, M. P.; Tildesley, D. J. *Computer Simulation of Liquids*; Clarendon Press: Oxford.
(29) Rojas, M. I. *Surf. Sci.* **2004**, *569*, 76−88.
(30) Trebst, S.; Huse, D. A.; Troyer, M. *Phys. Rev. E* **2004**, *70*, 046701.
(31) Berg, A. *Comput. Phys. Commun.* **2003**, *153*, 397−406.
(32) Hukushima, K.; Nemoto, K. *J. Phys. Soc. Jpn.* **1996**, *65*, 1604−1608.
(33) Wang, F.; Landau, D. P. *Phys. Rev. Lett.* **2001**, *86*, 2050−2053.
(34) Hesselbo, B.; Stinchcombe, R. B. *Phys. Rev. Lett.* **1995**, *74*, 2151−2155.
(35) Poulain, P.; Calvo, F.; Antoine, R.; Broyer, M.; Dugourd, Ph. *Phys. Rev. E* **2006**, *73*, 056704.
(36) Kim, J.; Straub, J. E.; Keyes, T. *J. Chem. Phys.* **2007**, *126*, 135101.
(37) Fenwick, M. K. *J. Chem. Phys.* **2008**, *129*, 125106.
(38) Alonso, J. A. *Structure and Properties of Atomic Nanoclusters*; Imperial College Press: London, 2005.
(39) Jellinek, J. *Theory of atomic and molecular clusters: with a glimpse at experiments*; Springer-Verlag: Berlin, 1999.
(40) Mottet, C.; Baletto, F.; Rossi, G.; Ferrando, R. *Phys. Rev. Lett.* **2005**, *95*, 035501−035504.
(41) Cheng, D. J.; Huang, S. P.; Wang, W. C. *Phys. Rev. B* **2006**, *74*, 064117−064127.
(42) Rossi, G.; Rapallo, A.; Mottet, C.; Fortunelli, A.; Baletto, F.; Ferrando, R. *Phys. Rev. Lett.* **2004**, *93*, 105503−105506.
(43) Calvo, S. R.; Balbuena, P. B. *Surf. Sci.* **2005**, *581*, 213−224.
(44) Lin, S. T.; Blanco, M.; Goddard, W., III *J. Chem. Phys.* **2003**, *119*, 11792−117805.
(45) Garzón, I. L.; Michaelian, K.; Beltrán, M. R.; Posada-Amarillas, A.; Ordejón, P.; Artacho, E.; Sánchez-Portal, D.; Soler, J. M. *Phys. Rev. Lett.* **1998**, *81*, 1600−1603.